

# Polarized line transfer with $F$ -state interference in a non-magnetic medium

*Partial frequency redistribution effects in the collisionless regime*

H. N. Smitha<sup>1</sup>, K. Sowmya<sup>1</sup>, K. N. Nagendra<sup>1</sup>, M. Sampoorna<sup>1</sup> and J. O. Stenflo<sup>2,3</sup>

<sup>1</sup>*Indian Institute of Astrophysics, Koramangala, Bangalore, India*

<sup>2</sup>*Institute of Astronomy, ETH Zurich, CH-8093 Zurich, Switzerland*

<sup>3</sup>*Istituto Ricerche Solari Locarno, Via Patocchi, 6605 Locarno-Monti, Switzerland*

smithahn@iiap.res.in; ksowmya@iiap.res.in; knn@iiap.res.in; sampoorna@iiap.res.in;  
stenflo@astro.phys.ethz.ch

## ABSTRACT

Quantum interference phenomena manifests itself in several ways in the polarized solar spectrum formed due to coherent scattering processes. One such effect arises due to interference between the fine structure ( $J$ ) states giving rise to multiplets. Another effect is that which arises due to interference between the hyperfine structure ( $F$ ) states. We extend the redistribution matrix derived for the  $J$ -state interference to the case of  $F$ -state interference. We then incorporate it into the polarized radiative transfer equation and solve it for isothermal constant property slab atmospheres. The relevant transfer equation is solved using a polarized approximate lambda iteration (PALI) technique based on operator perturbation. An alternative method derived from the Neumann series expansion is also proposed and is found to be relatively more efficient than the PALI method. The effects of PRD and the  $F$ -state interference on the shapes of the linearly polarized Stokes profiles are discussed. The emergent Stokes profiles are computed for hypothetical line transitions arising due to hyperfine structure splitting (HFS) of the upper  $J = 3/2$  and lower  $J = 1/2$  levels of a two-level atom model with nuclear spin  $I_s = 3/2$ . We confine our attention to the non-magnetic scattering in the collisionless regime.

*Subject headings:* line: formation – methods: numerical – polarization – radiative transfer – scattering – Sun: atmosphere

## 1. Introduction

The linearly polarized solar spectrum is produced by coherent scattering processes taking place in the solar atmosphere. This so called ‘second solar spectrum’ is highly structured and reveals various physical processes responsible to generate the polarized signals in the spectrum. Quantum interference is one such physical process whose importance has been highlighted in the second solar spectrum studies (see Stenflo 1980, 1994, 1997). The coherent superposition of the fine structure states leads to the  $J$ -state interference, whereas the  $F$ -state interference arises due to superposition of the hyperfine structure states

(see Figure 1). The  $J$ -state interference theory for the case of frequency coherent scattering was developed by Stenflo (1980, 1994, 1997). This theory was extended to include partial frequency redistribution (PRD) in line scattering, by Smitha et al. (2011a, hereafter called P1). The  $J$ -state PRD matrix derived in P1 is used in the polarized line transfer equation in Smitha et al. (2011b, hereafter P2). An alternative scattering theory of  $J$ -state interference based on metalevel approach was developed by Landi Degl’Innocenti et al. (1997), which also includes the  $F$ -state interference effects. All the papers mentioned so far are applicable to the case of collisionless regime.

Second solar spectrum contains several lines which have signatures of  $F$ -state interference. Examples of these lines are Na I D<sub>2</sub> at 5890 Å, Ba II D<sub>2</sub> at 4554 Å, Mn I 8741 Å, Sc II 4247 Å etc. In this paper we are concerned with the line formation studies involving  $F$ -state interference process and PRD. The  $F$ -state redistribution matrix derived in this paper can be used for modeling the non-magnetic quiet region observations of hyperfine structure splitting (HFS) in the lines mentioned above.

The  $F$ -state interference theory applicable to the frequency coherent scattering was developed by Stenflo (1997). This theory, along with PRD, was applied by Fluri et al. (2003) and Holzreuter et al. (2005) in the polarized line transfer computations. In Landi Degl'Innocenti & Landolfi (2004) the theory of  $F$ -state interference was developed under the approximation of complete frequency redistribution (CRD). The theory of  $F$ -state interference in a magnetic field for multi-term atoms in the collisionless regime and under the approximation of CRD is presented in Casini & Manso Sainz (2005).

In the present paper we extend the  $J$ -state interference theory presented in P1 to the case of  $F$ -state interference. The  $F$ -state redistribution matrix is derived here for the non-magnetic case and in the collisionless regime. The reason for considering the non-magnetic case in this paper, is that the formulation of P1 was confined to the linear Zeeman regime of field strengths (the spacing between the Zeeman  $m$ -states being smaller than the spacing between the fine structure states). In the present context, the hyperfine splitting becomes comparable to the Zeeman splitting even for weak magnetic fields, and we quickly enter the Paschen-Back regime of field strengths (level crossing of the  $m$ -states belonging to different  $F$ -states), in which the formulation presented in P1 is not valid. Since the Paschen-Back effect is outside the scope of the present paper, our treatment here is limited to the non-magnetic case, but the extension to the Paschen-Back regime is planned to be pursued in future work. We further assume that the lower level is unpolarized and infinitely sharp. While this assumption is made for the sake of mathematical simplicity, it is physically justified for the long-lived ground states, which are correspondingly more vulnerable to collisional depolarization.

Following P2, this PRD matrix is incorporated into the polarized line transfer equation, and solved using an operator perturbation method. We also propose a new method to solve the  $F$ -state interference problem. It is called the scattering expansion method (SEM) and is described in Frisch et al. (2009); Sampooran et al. (2011). Recently it has been applied to a variety of problems (see Sowmya et al. 2012; Supriya et al. 2012). We compare the operator perturbation method and the SEM by applying them to the problem at hand.

In Section 2 we derive the PRD matrix for  $F$ -state interference and incorporate it into the line transfer equation. In Section 3 we describe the numerical methods used to solve the transfer equation. Results are presented in Section 4. Section 5 is devoted to the concluding remarks.

## 2. Basic equations

### 2.1. The redistribution matrix

In this section we present the redistribution matrix for the  $F$ -state interference, derived starting from the Kramers-Heisenberg formula. We restrict our attention to the case of non-magnetic collisionless regime.

The redistribution matrix for the  $F$ -state interference can be derived through a straight forward replacement of quantum numbers, in the  $J$ -state interference redistribution matrix derived in P1. The replacements are as follows (see Stenflo 1997; Landi Degl'Innocenti & Landolfi 2004):

$$L \rightarrow J; \quad J \rightarrow F; \quad S \rightarrow I_s, \quad (1)$$

where  $L$ ,  $J$  and  $S$  represent the orbital, electronic, and spin quantum numbers of a given state.  $F$  is the total angular momentum and  $I_s$  the nuclear

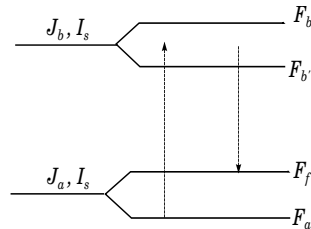


Fig. 1.— Level diagram representing the HFS in a two-level atom model.

spin of the atom under consideration. The expression for the  $F$ -state interference redistribution matrix expressed in terms of irreducible spherical tensors can be written as

$$\begin{aligned} \mathbf{R}_{ij}^{\text{II}}(x, \mathbf{n}; x', \mathbf{n}') &= \frac{3(2J_b + 1)}{2I_s + 1} \\ &\times \sum_{KF_a F_f F_b F_{b'}} (-1)^{F_f - F_a} \cos \beta_{F_{b'}, F_b} e^{i\beta_{F_{b'}, F_b}} \\ &\times \left[ (h_{F_b, F_{b'}}^{\text{II}})_{F_a F_f} + i(f_{F_b, F_{b'}}^{\text{II}})_{F_a F_f} \right] \\ &\times (2F_a + 1)(2F_f + 1)(2F_b + 1)(2F_{b'} + 1) \\ &\times \begin{Bmatrix} J_a & J_b & 1 \\ F_b & F_f & I_s \end{Bmatrix} \begin{Bmatrix} J_a & J_b & 1 \\ F_b & F_a & I_s \end{Bmatrix} \\ &\times \begin{Bmatrix} J_a & J_b & 1 \\ F_{b'} & F_f & I_s \end{Bmatrix} \begin{Bmatrix} J_a & J_b & 1 \\ F_{b'} & F_a & I_s \end{Bmatrix} \\ &\times \begin{Bmatrix} 1 & 1 & K \\ F_{b'} & F_b & F_a \end{Bmatrix} \begin{Bmatrix} 1 & 1 & K \\ F_{b'} & F_b & F_f \end{Bmatrix} \\ &\times \mathcal{T}_0^K(i, \mathbf{n}) \mathcal{T}_0^K(j, \mathbf{n}'). \end{aligned} \quad (2)$$

In the above expression the angle  $\beta_{F_{b'}, F_b}$  is defined as

$$\tan \beta_{F_{b'}, F_b} = \frac{\omega_{F_{b'}, F_b}}{\gamma}, \quad (3)$$

where  $\hbar\omega_{F_{b'}, F_b}$  represent the energy differences between the  $F_{b'}$  and  $F_b$  states in the absence of a magnetic field.  $\gamma$  is the damping parameter of the upper state. The lower levels are assumed to be infinitely sharp and unpolarized. The  $h$  and  $f$  functions are the auxiliary quantities defined in the same way as Equations (14) - (15) of P1, but with the replacements given in Equation (1).  $\mathcal{T}_Q^K$  are the irreducible tensors for polarimetry introduced by Landi Degl'Innocenti (1984). For the non-magnetic case presented in this paper  $Q = 0$ . The indices  $i$  and  $j$  refer to the Stokes parameters ( $i, j = 0, 1, 2, 3$ ) with  $K = 0, 1, 2$  and  $-K \leq Q \leq +K$ . The directions of the incoming and scattered rays are given by  $\mathbf{n}'$  and  $\mathbf{n}$  respectively.  $\mathbf{n} = (\theta, \varphi)$  with  $\theta$  being the colatitude and  $\varphi$  being the azimuth of the outgoing ray.  $x'$  and  $x$  are the incoming and scattered frequencies in Doppler width units.

## 2.2. The polarized line transfer equation

The one dimensional radiative transfer equation for solving the line formation problems with PRD and  $F$ -state interference in scattering in the ab-

sence of a magnetic field is given by

$$\mu \frac{\partial \mathbf{I}(\tau, x, \mu)}{\partial \tau} = (\phi_{\text{HFS}}(x) + r) [\mathbf{I}(\tau, x, \mu) - \mathbf{S}(\tau, x, \mu)], \quad (4)$$

where  $\mathbf{I} = (I, Q)^T$  is the Stokes vector and  $\mathbf{S} = (S_I, S_Q)^T$  is the Stokes source vector. Equation (4) is valid for the case of a two-level atom with an infinitely sharp and unpolarized ground level.  $\mu = \cos \theta$  represents the line of sight.  $r$  is the ratio of continuum to the frequency-integrated line absorption coefficient. The positive Stokes  $Q$  represents electric vector vibrations perpendicular to the solar limb.  $\tau$  is the line optical depth defined by  $d\tau = -k_L dz$ , where  $k_L$  is the frequency-integrated line absorption coefficient defined for a two-level atom with HFS. If  $\eta_L$  is the line absorption coefficient then for the standard two-level atom without HFS,  $\eta_L = k_L \phi(x)$  where  $\phi(x)$  is the Voigt profile function. In the presence of HFS,  $\eta_L$  is given by (see Equation (7) of P2)

$$\begin{aligned} \eta_L(\nu) &= \frac{k_L}{(2I_s + 1)} \sum_{F_a F_b} (2F_a + 1)(2F_b + 1) \\ &\times \left\{ \begin{Bmatrix} J_b & J_a & 1 \\ F_a & F_b & I_s \end{Bmatrix} \right\}^2 \phi(\nu_{F_b F_a} - \nu), \end{aligned} \quad (5)$$

where

$$k_L = \frac{\hbar \nu_{J_b J_a}}{4\pi} N(J_a) B(J_a \rightarrow J_b), \quad (6)$$

is the frequency-integrated absorption coefficient for all the  $F$ -states. Thus  $\phi_{\text{HFS}}(x)$  is the weighted sum of the individual Voigt profiles  $\phi(\nu_{F_b F_a} - \nu)$  representing each of the  $F_a \rightarrow F_b$  absorption.

For the particular case of  $J_a = 1/2 \rightarrow J_b = 3/2 \rightarrow J_f = 1/2$  transition with  $I_s = 3/2$ ,  $\phi_{\text{HFS}}(x)$  takes the form

$$\begin{aligned} \phi_{\text{HFS}}(x) &= \left[ \frac{2}{32} \phi(\nu_{01} - \nu) + \frac{5}{32} \phi(\nu_{11} - \nu) \right. \\ &+ \frac{5}{32} \phi(\nu_{21} - \nu) + \frac{1}{32} \phi(\nu_{12} - \nu) \\ &\left. + \frac{5}{32} \phi(\nu_{22} - \nu) + \frac{14}{32} \phi(\nu_{32} - \nu) \right]. \end{aligned} \quad (7)$$

We have verified that if the  $F$ -states are very closely spaced, then a single profile function  $\phi(\nu_{J_b J_a} - \nu)$ , corresponding to the  $J_a \rightarrow J_b$  transition, can be used instead of  $\phi_{\text{HFS}}(x)$  (see Landi Degl'Innocenti & Landolfi 2004).

The total source vector  $\mathbf{S}$  in Equation (4) is given by

$$\mathbf{S}(\tau, x, \mu) = \frac{\phi_{\text{HFS}}(x)\mathbf{S}_l(\tau, x, \mu) + r\mathbf{S}_c}{\phi_{\text{HFS}}(x) + r}, \quad (8)$$

where the unpolarized continuum source vector  $\mathbf{S}_c = B\mathbf{U}$ , with  $B$  being the Planck function and  $\mathbf{U} = (1, 0)^T$ . The line source vector for a two-level atom with HFS is given by

$$\begin{aligned} \mathbf{S}_l(\tau, x, \mu) &= \epsilon B\mathbf{U} + \frac{1}{\phi_{\text{HFS}}(x)} \int_{-\infty}^{+\infty} dx' \\ &\times \int_{-1}^{+1} \frac{d\mu'}{2} \mathbf{R}(x, \mu; x', \mu') \mathbf{I}(\tau, x', \mu'). \end{aligned} \quad (9)$$

Here  $\epsilon = \Gamma_I/(\Gamma_I + \Gamma_R)$  is the photon destruction probability per scattering also known as the thermalization parameter, with  $\Gamma_I$  and  $\Gamma_R$  being the inelastic and radiative de-excitation rates of the upper state  $F_b$ . To a first approximation these rates are assumed to be the same for all the  $F$ -states.  $\mathbf{R}(x, \mu; x', \mu')$  is the redistribution matrix defined in Equation (2) but integrated over the azimuths  $\varphi'$  of the incoming radiation. Such a simplification is possible due to the azimuthal symmetry of the problem. This redistribution matrix can be rewritten as

$$\begin{aligned} \mathbf{R}_{ij}(x, \mu; x', \mu') &= \sum_K \mathcal{R}^K(x, x') \\ &\times \mathcal{T}_0^K(i, \mu) \mathcal{T}_0^K(j, \mu'). \end{aligned} \quad (10)$$

The redistribution function components  $\mathcal{R}^K(x, x')$  are given by

$$\begin{aligned} \mathcal{R}^K(x, x') &= \frac{3(2J_b + 1)}{2I_s + 1} \sum_{F_a F_f F_b F_{b'}} (-1)^{F_f - F_a} \\ &\times \cos \beta_{F_b', F_b} [\cos \beta_{F_b', F_b} (h_{F_b, F_{b'}}^{\text{II}})_{F_a F_f} \\ &- \sin \beta_{F_b', F_b} (f_{F_b, F_{b'}}^{\text{II}})_{F_a F_f}] \\ &\times (2F_a + 1)(2F_f + 1)(2F_b + 1)(2F_{b'} + 1) \\ &\times \begin{Bmatrix} J_a & J_b & 1 \\ F_b & F_f & I_s \end{Bmatrix} \begin{Bmatrix} J_a & J_b & 1 \\ F_b & F_a & I_s \end{Bmatrix} \\ &\times \begin{Bmatrix} J_a & J_b & 1 \\ F_{b'} & F_f & I_s \end{Bmatrix} \begin{Bmatrix} J_a & J_b & 1 \\ F_{b'} & F_a & I_s \end{Bmatrix} \\ &\times \begin{Bmatrix} 1 & 1 & K \\ F_{b'} & F_b & F_a \end{Bmatrix} \begin{Bmatrix} 1 & 1 & K \\ F_{b'} & F_b & F_f \end{Bmatrix}. \end{aligned} \quad (11)$$

For simplicity, we use the angle-averaged versions of the auxiliary functions  $(h_{F_b, F_{b'}}^{\text{II}})_{F_a F_f}$  and  $(f_{F_b, F_{b'}}^{\text{II}})_{F_a F_f}$ .

### 2.3. Decomposition of the Stokes vectors into the reduced basis

Decomposition of the Stokes source vector  $\mathbf{S}$  in the reduced basis makes it independent of  $\theta$ . The decomposition of  $\mathbf{S}$  defined in Equation (8) can be carried out in a way similar to the one presented in Section 2.1 of P2. Hence we do not repeat them here. The transfer equation for the reduced Stokes vector  $\mathcal{I}$  can be written as

$$\mu \frac{\partial \mathcal{I}(\tau, x, \mu)}{\partial \tau} = (\phi_{\text{HFS}}(x) + r)[\mathcal{I}(\tau, x, \mu) - \mathbf{S}(\tau, x)]. \quad (12)$$

The corresponding irreducible total and line source vectors are given by

$$\mathbf{S}(\tau, x) = \frac{\phi_{\text{HFS}}(x)\mathbf{S}_l(\tau, x) + r\mathcal{G}(\tau)}{\phi_{\text{HFS}}(x) + r}, \quad (13)$$

and

$$\mathbf{S}_l(\tau, x) = \epsilon \mathcal{G}(\tau) + \int_{-\infty}^{+\infty} \frac{\tilde{\mathcal{R}}(x, x')}{\phi_{\text{HFS}}(x)} \mathcal{J}(\tau, x') dx'. \quad (14)$$

Here  $\tilde{\mathcal{R}}(x, x')$  is a  $(2 \times 2)$  diagonal matrix with elements  $\tilde{\mathcal{R}} = \text{diag}(\mathcal{R}^0, \mathcal{R}^2)$ , where  $\mathcal{R}^K$  are defined in Equation (11).  $\mathcal{G}(\tau) = (B, 0)^T$  is the primary source vector, and  $\mathcal{J}(\tau, x)$  is the mean intensity defined in Equation (22) of P2.

### 3. The numerical methods

Here we describe two numerical techniques to solve the reduced form of the transfer equation. We compare their performance on some benchmark problems.

#### 3.1. Operator perturbation method

The solution of the polarized line transfer equation defined in Equation (12) using the polarized approximate lambda iteration (PALI) method is described in Sections 3.1 and 3.2 of P2. The same equations hold good for the present problem also. Hence we do not repeat those equations here. The only difference is that the redistribution matrix for  $J$ -state interference is now to be replaced by the corresponding redistribution matrix for the  $F$ -state interference presented in this paper. Also the profile function is to be replaced with  $\phi_{\text{HFS}}(x)$ .

### 3.2. Scattering expansion method

In recent years a new method based on Neumann series expansion of the polarized source vector has been developed (see Frisch et al. 2009). It is applied to a variety of astrophysical problems. Here we describe the application of this method to the problem at hand.

In this method, the reduced line source vector defined in Equation (14) is rewritten in the component form for the non-magnetic case as

$$S_0^K(\tau, x) = G(\tau)\delta_{K0}\delta_{00} + \int_{-1}^{+1} \frac{d\mu'}{2} \times \int_{-\infty}^{+\infty} dx' \frac{\mathcal{R}^K(x, x')}{\phi_{\text{HFS}}(x)} \sum_{K'} \Psi_0^{KK'}(\mu') I_0^{K'}(\tau, x', \mu'). \quad (15)$$

$\Psi_0^{KK'}$  are the components of the Rayleigh phase matrix in the reduced basis (see Appendix A of Frisch 2007). We first consider the component  $S_0^0$ . Expanding the summation over  $K'$  on the right-hand side of Equation (15) we obtain

$$S_0^0(\tau, x) = G(\tau) + \int_{-1}^{+1} \frac{d\mu'}{2} \int_{-\infty}^{+\infty} dx' \frac{\mathcal{R}^0(x, x')}{\phi_{\text{HFS}}(x)} \Psi_0^{00}(\mu') I_0^0(\tau, x', \mu') + \int_{-1}^{+1} \frac{d\mu'}{2} \int_{-\infty}^{+\infty} dx' \frac{\mathcal{R}^2(x, x')}{\phi_{\text{HFS}}(x)} \Psi_0^{02}(\mu') I_0^2(\tau, x', \mu'). \quad (16)$$

The degree of linear polarization arising due to Rayleigh scattering is small because of small degree of anisotropy prevailing in the solar atmosphere. Hence the effect of linear polarization on Stokes  $I$  can be neglected to a good approximation. Neglecting the contribution from  $I_0^2$ , in Equation (16) we get

$$\tilde{S}_0^0(\tau, x) \simeq G(\tau) + \int_{-1}^{+1} \frac{d\mu'}{2} \times \int_{-\infty}^{+\infty} dx' \frac{\mathcal{R}^0(x, x')}{\phi_{\text{HFS}}(x)} \Psi_0^{00}(\mu') I_0^0(\tau, x', \mu'), \quad (17)$$

where  $\tilde{S}_0^0$  denotes the approximate value of  $S_0^0$ . It is the solution of a non-LTE unpolarized radiative transfer equation and is computed using the Frequency-by-Frequency (FBF) technique of Paletou & Auer (1995).

The polarization is computed from the higher order terms in the series expansion. The  $S_0^2$  com-

ponent is given by

$$\tilde{S}_0^2(\tau, x) \simeq \int_{-1}^{+1} \frac{d\mu'}{2} \int_{-\infty}^{+\infty} dx' \frac{\mathcal{R}^2(x, x')}{\phi_{\text{HFS}}(x)} \times \Psi_0^{20}(\mu') \tilde{I}_0^0(\tau, x', \mu') + \int_{-1}^{+1} \frac{d\mu'}{2} \int_{-\infty}^{+\infty} dx' \frac{\mathcal{R}^2(x, x')}{\phi_{\text{HFS}}(x)} \times \Psi_0^{22}(\mu') \tilde{I}_0^2(\tau, x', \mu'). \quad (18)$$

Retaining only the contribution from  $\tilde{I}_0^0$  on the right-hand side of Equation (18) we obtain the single scattering approximation to the polarized component of the source vector as

$$[\tilde{S}_0^2(\tau, x)]^{(1)} \simeq \int_{-1}^{+1} \frac{d\mu'}{2} \int_{-\infty}^{+\infty} dx' \frac{\mathcal{R}^2(x, x')}{\phi_{\text{HFS}}(x)} \times \Psi_0^{20}(\mu') \tilde{I}_0^0(\tau, x', \mu'). \quad (19)$$

The superscript (1) denotes single (first) scattering. This solution serves as a starting point for the computations of higher order scattering terms. Thus the iterative sequence of SEM can be represented by

$$[\tilde{S}_0^2(\tau, x)]^{(n)} \simeq [\tilde{S}_0^2(\tau, x)]^{(1)} + \int_{-1}^{+1} \frac{d\mu'}{2} \int_{-\infty}^{+\infty} dx' \frac{\mathcal{R}^2(x, x')}{\phi_{\text{HFS}}(x)} \times \Psi_0^{22}(\mu') [\tilde{I}_0^2(\tau, x', \mu')]^{(n-1)}, \quad (20)$$

where the superscript  $(n)$  denotes the  $n^{\text{th}}$  scattering. The iterative cycle is continued until the required convergence criteria is met.

In the following we compare the performance of these two numerical methods by plotting the maximum relative correction defined as

$$c^{(n)} = \max\{c_1^{(n)}, c_2^{(n)}\} < 10^{-8}, \quad (21)$$

where

$$c_1^{(n)} = \max_{\tau, x, \mu} \left\{ \frac{|\delta S_I^{(n)}(\tau, x, \mu)|}{|\bar{S}_I^{(n)}(\tau, x, \mu)|} \right\}, \quad (22)$$

and

$$c_2^{(n)} = \max_{x, \mu} \left\{ \frac{P^{(n)}(x, \mu) - P^{(n-1)}(x, \mu)}{P^{(n-1)}(x, \mu)} \right\}, \quad (23)$$

as a function of the iteration number as shown in Figure 2. In the above equations  $P = [Q/I]$  is the

degree of linear polarization and  $\bar{S}_I^{(n)} = \frac{1}{2}[S_I^{(n)} + S_I^{(n-1)}]$ .

Figure 2 is computed for a test problem defined by the model parameters  $(T, a, \epsilon, r, B) = (2 \times 10^{10}, 2 \times 10^{-3}, 10^{-4}, 0, 1)$  where  $T$  is the optical thickness of the self emitting slab and  $a$  is the damping parameter of the upper level  $J_b$ . From the figure one can clearly see that the convergence rate of the SEM is larger by several factors compared to the PALI method. The reason for the PALI method being slow is that the source function corrections are computed iteratively from an approximate initial guess and then the approximate lambda operator is perturbed until the source function corrections fall below a convergence criteria. On the other hand, the initial guess in the SEM for polarized line formation is the single scattered solution itself (which already contains the physical characteristics of the scattering mechanism under consideration). For this reason SEM takes just a few iterations to converge to the same level of accuracy as the PALI method. Further, SEM is easy to implement for problems of any physical and/or numerical complexity. This makes the SEM a method of choice. For a detailed comparison of PALI and SEM we refer to Sampoorana et al. (2011) and Supriya et al. (2012). The simple Lambda iteration for polarization and the SEM are essentially similar. In the lambda iteration, a source vector correction is computed at each iteration, and the current source vector is updated until convergence is reached. In the SEM, each iteration can be seen as contributing a higher order scattering term to the series expansion of polarized component of the source vector. This component is updated by adding successively higher order terms in the scattering expansion of the source vector. These points are clearly explained respectively in Trujillo Bueno & Manso Sainz (1999, see the discussion following their Equation (28)), and Frisch et al. (2009, see the discussion following their Equation (36)).

## 4. Results and discussion

In this section we present the results computed for a standard two-level atom model with  $F$ -state interference using the PRD matrix presented in this paper. Isothermal constant property media

characterized by  $(T, a, \epsilon, r, B)$  are used. The slabs are assumed to be self-emitting.

The results are presented for transitions centered at hypothetical wavelengths arising due to HFS of the  $J_b = 3/2$  and  $J_a = 1/2$  levels of a two-level atom with nuclear spin  $I_s = 3/2$ . Due to the hyperfine interactions the upper  $J$ -state splits into four  $F$ -states with  $F_b = 0, 1, 2, 3$ , and the lower  $J$ -state splits into  $F_a = 1, 2$ . Owing to the selection rule  $\Delta F = 0, \pm 1$ , these  $F$ -states produce six radiative transitions involving them (see Table 1). For simplicity the Doppler width of all the lines is taken to be constant at  $\Delta\lambda_D = 25$  mÅ. In the transfer computations, a grid resolution of  $(N_d, N_x, N_\mu) = (5, 417, 5)$  is generally used, where  $N_d$  is the number of depth points per decade in the logarithmically spaced  $\tau$ -grid. The first depth point is taken as  $\tau_{\min} = 10^{-2}$ .  $N_x$  is the total number of frequency points covering the full line profile.  $N_\mu$  is the number of co-latitudes  $\theta(\mu)$ , taken as the 5 points of a Gauss-Legendre quadrature.

### 4.1. $F$ -state interference effects in the case of single scattering

In this section we study the behavior of the  $F$ -state interference PRD matrix derived in Section 2.1 by computing the scattered profiles in a single scattering event. The results in Figure 3 are computed for a  $90^\circ$  single scattering event. This is done by giving as input an unpolarized beam of light incident on the scattering atom at  $\mu' = -1$  and observing the scattered ray at  $\mu = 0$  in the scattering plane (see P1 for details on computing polarization profiles in a  $90^\circ$  single scattered event). The dashed line in Figure 3 is computed by ignoring the interference effects, whereas the solid line is computed by taking account of the interference effects between the  $F$ -states. Profile similar to the solid line can also be seen in Fluri et al. (2003) and Holzreuter et al. (2005) where plots of the wavelength dependent polarizability factor  $W_2(\lambda)$  are shown. In the single scattering case, the profiles of the  $W_2(\lambda)$  and the  $Q(\lambda)/I(\lambda)$  are similar in shape but differ only in magnitude (see below).

#### 4.1.1. Principle of spectroscopic stability for $F$ -state interference

It is well known that the principle of spectroscopic stability provides a useful tool to check any theory of quantum interference. This was first discussed in the context of scattering polarization and applied in detail in Stenflo (1994) (see also Stenflo 1997; Landi Degl’Innocenti & Landolfi 2004). In this paper, we apply it to the case of  $F$ -state interference arising due to the nuclear spin  $I_s$ . According to the principle of spectroscopic stability, in the limit of vanishing HFS in a two-level atom, the theory of  $F$ -state interference should reduce to the standard two-level atom theory without HFS. This can be verified by computing the polarizability factor  $W_2$  and in turn the fractional polarization  $Q/I$  in the limit of vanishing  $F$ -states. The value of  $W_2$  in this asymptotic limit (which can be obtained by neglecting the  $I_s$ ) can be computed as described in Stenflo (1997) with

$$(W_2)_{\text{asym}} = \frac{\begin{Bmatrix} 1 & 1 & 2 \\ J_b & J_b & J_a \end{Bmatrix} \begin{Bmatrix} 1 & 1 & 2 \\ J_b & J_b & J_f \end{Bmatrix}}{\begin{Bmatrix} 1 & 1 & 0 \\ J_b & J_b & J_a \end{Bmatrix} \begin{Bmatrix} 1 & 1 & 0 \\ J_b & J_b & J_f \end{Bmatrix}}. \quad (24)$$

For the particular case of  $J_a = 1/2 \rightarrow J_b = 3/2 \rightarrow J_f = 1/2$  scattering transition,  $(W_2)_{\text{asym}} = 0.5$ . Hence  $W_2(\lambda)$  is expected to approach 0.5 in the very far wings (see Figure 2 of Stenflo 1997). In the  $90^\circ$  single scattering case, the  $Q/I$  and the  $W_2(\lambda)$  are related through the formula (see Landi Degl’Innocenti & Landolfi 2004)

$$Q(\lambda)/I(\lambda) = \frac{3W_2(\lambda)}{4 - W_2(\lambda)}. \quad (25)$$

The above formula gives in the far wings a value of  $Q/I = 0.428$  for  $(W_2)_{\text{asym}} = 0.5$ .

From Figure 3, we can see that the solid curve reaches an asymptotic value of 42.8% as demanded by the principle of spectroscopic stability, whereas the dashed line reaches about 10% in the far wings, thereby violating the principle of spectroscopic stability. These arguments show that in the formulation of the redistribution matrix, the inclusion of interference effects between the  $F$ -states is essential.

#### 4.2. Effects of $F$ -state interference in multiply scattered Stokes profiles

In this section we present the results obtained by solving the transfer equation including the  $F$ -state interference. In the particular case of optically thin slabs, it can be shown, by choosing appropriate geometric arrangement, that the multiply scattered solution approaches single scattered solution thus proving that we have correctly incorporated the  $F$ -state redistribution matrix in the line transfer code. See P2 for more details regarding single scattering in a thin atmospheric slab.

When the optical thickness of the medium is large, multiple scattering effects come into play. Figure 4 shows one such example, where the emergent Stokes profiles are computed for different optical thicknesses. The dashed line in this figure is computed by neglecting HFS. This is the standard two-level atom case which results in a single radiative transition. The dotted line is computed with HFS but without interference between the  $F$ -states. In this case the six radiative transitions arising due to HFS are treated independently. The solid line is computed taking account of the  $F$ -state interference. This comprises of six interfering radiative transitions between the  $F$ -states. The three line types in this figure are quite similar to each other in shape but differ prominently in amplitude.

For  $T = 2$ , the atmospheric slab is effectively thin and the  $Q/I$  profiles for both solid and dotted lines have a structuring within the line core which is different from that of the dashed line. This is due to the HFS of the given  $J$ -level. As the optical thickness increases, such a structuring gets smoothened out and the shape (not the amplitude) of the solid and dotted line profiles resemble more closely with the dashed line profiles.

In the case of effectively thick atmospheric slabs ( $T > 2$ ), two peaks are seen on either side of the line center arising due to PRD effects and are known as PRD wing peaks. In the line core, the solid and dotted lines nearly coincide whereas the dashed line differs from these two. This shows that the depolarization in the line core is purely due to HFS, irrespective of the interference effects between the  $F$ -states being included. In the wings, the solid line and the dashed line coincide whereas the dotted line differs significantly. Upon compar-

ing the solid and dotted lines, it is evident that the interference effects show up in the line wing PRD peaks like in the case of  $J$ -state interference. However the  $J$ -state interference effects are seen even beyond the PRD wing peaks unlike the case of  $F$ -state interference. When  $F$ -state interference is taken into account the  $Q/I$  in the wings reaches the value of the single line case as expected from the principle of spectroscopic stability (see Section 4.1.1). But when interference is neglected, the dotted and dashed lines differ considerably in the wings which can be seen as a violation of the principle of spectroscopic stability. Thus the principle of spectroscopic stability serves as a powerful tool to check the correctness of our formulation not only in the case of single scattering but also in the radiative transfer computations.

Though such significant signatures of HFS and  $F$ -state interference are seen in  $Q/I$ , the intensity  $I$  remains unaffected by these effects.

#### 4.3. Comparison with wavelength dependent polarizability theory of Stenflo

In this section we compare our redistribution matrix approach and the wavelength dependent polarizability  $W_2(\lambda)$  theory for the case of  $F$ -state interference presented in Stenflo (1997) and used in Fluri et al. (2003) and Holzreuter et al. (2005). The comparison is shown in Figure 5. The dotted lines show the profiles computed using the exact PRD  $F$ -state interference theory presented in Section 2. This is our redistribution matrix approach. The dashed lines show the profiles computed using the  $W_2(\lambda)$  approach. The values of the  $W_2(\lambda)$  are calculated from Equation (25) using the  $(Q/I)$  plotted in Figure 3 (solid line). To use the  $W_2(\lambda)$  in radiative transfer computations we replace the redistribution matrix  $\mathcal{R}^K(x, x')$  in Equation (11) by

$$W_K(\lambda)[R^{\text{II-A}}(3/2 \rightarrow 1/2)], \quad (26)$$

where  $R^{\text{II-A}}(J_b \rightarrow J_f)$  is the angle-averaged frequency redistribution function of Hummer (1962) for a line centered at  $\lambda_{J_b J_f}$  corresponding to the  $J_b \rightarrow J_f$  transition. For the hypothetical case under study, we have assumed the  $F$ -states to be very closely spaced. Under such an assumption, a single redistribution function computed for the  $J = 3/2 \rightarrow 1/2$  transition can be used to represent all the  $F$ -state transitions. However if

the  $F$ -states are far apart then the redistribution function needs to be computed for each of the  $F_b \rightarrow F_f$  transition. In such a case, the redistribution matrix  $\mathcal{R}^K(x, x')$  takes the following form in the  $W_2(\lambda)$  approach:

$$W_K(\lambda) \sum_{F_b F_f} [R^{\text{II-A}}(F_b \rightarrow F_f)]. \quad (27)$$

The polarizability factor  $W_0(\lambda) = 1$ , and  $W_2(\lambda)$  is the wavelength-dependent  $W_2$  factor calculated from Equation (25). For the closely spaced  $F$ -states a common absorption profile function  $\phi(x)$  corresponding to the  $J_a = 1/2 \rightarrow J_b = 3/2$  transition is used. But in the case of widely spaced  $F$ -states, the  $\phi(x)$  has to be taken as the sum of all the individual  $F_a \rightarrow F_b$  absorption profile functions. As seen from Figure 5 both the redistribution matrix approach and the  $W_2(\lambda)$  approach give nearly the same results.

#### 5. Conclusions

In the present paper we have extended the  $J$ -state interference formulation discussed in P1 and P2 to the case of  $F$ -state interference. The treatment is restricted to the collisionless and non-magnetic regime. The decomposition technique presented in Frisch (2007) is applied to the  $F$ -state interference problem. It helps to incorporate the  $F$ -state interference redistribution matrix into the reduced form of the line radiative transfer equation. The transfer equation is solved using the traditional PALI and the scattering expansion method by suitably adapting them to handle the  $F$ -state interference problem. The SEM is found to be more efficient and faster than the PALI method.

The Stokes profiles computed by taking account of HFS are similar to the profiles of a single line arising from a two-level atom model without HFS. The HFS causes a depolarization of  $Q/I$  in the line core irrespective of whether the  $F$ -state interference is taken into account or not. Like the  $J$ -state interference, the  $F$ -state interference affects mainly the line wing PRD peaks. We also show that when interference effects are neglected, the principle of spectroscopic stability is violated in both single scattered and multiple scattered profiles. Using the fractional polarization  $Q/I$  in the  $90^\circ$  single scattering case, we can numerically esti-



mate the wavelength dependent polarizability factor  $W_2(\lambda)$ . The  $W_2(\lambda)$  so computed can then be used in the transfer equation to compare with our exact redistribution matrix approach. The two approaches are found to give identical emergent Stokes profiles.

## REFERENCES

- Casini, R., & Manso Sainz, R. 2005 ApJ, 624, 1025
- Fluri, D. M., Holzreuter, R., Klement, J., & Stenflo, J. O. 2003, in ASP Conf. Ser. 307, Solar Polarization III, ed. J. Trujillo-Bueno & J. Sánchez Almeida (San Francisco, CA: ASP), 263
- Frisch, H. 2007, A&A, 476, 665
- Frisch, H., Anusha, L. S., Sampoorana, M. & Nagendra, K. N. 2009, A&A, 501, 335
- Holzreuter, R., Fluri, D. M., & Stenflo J.O. 2005, A&A, 434, 713
- Hummer, D. G. 1962, MNRAS, 125, 21
- Landi Degl’Innocenti E. 1984, Sol. Phys., 91, 1
- Landi Degl’Innocenti, E., Landi Degl’Innocenti, M., & Landolfi, M. 1997, in Proc. Forum THÉMIS, Science with THÉMIS, ed. N. Mein & S. Sahal-Bréchet (Paris: Obs. Paris-Meudon), 59
- Landi Degl’Innocenti, E., & Landolfi, M. 2004, Polarization in Spectral Lines (Dordrecht: Kluwer)
- Paletou, F., & Auer, L. H. 1995, A&A, 297, 771
- Sampoorana, M., Nagendra, K. N., & Frisch, H. 2011, A&A, 527, A89
- Smitha, H. N., Sampoorana, M., Nagendra, K. N., & Stenflo, J. O. 2011a, ApJ, 733, 4 (P1)
- Smitha, H. N., Nagendra, K. N., Sampoorana, M., & Stenflo, J. O. 2011b, A&A, 535, 35 (P2)
- Sowmya, K., Nagendra, K. N., & Sampoorana, M., 2012, MNRAS, 423, 2949
- Stenflo, J. O. 1980, A&A, 84, 68
- Stenflo, J. O. 1994, Solar Magnetic Fields: Polarized Radiation Diagnostics (Dordrecht: Kluwer)
- Stenflo, J. O. 1997, A&A, 324, 344
- Supriya, H. D., Nagendra, K. N., Sampoorana, M., & Ravindra, B. 2012, MNRAS, 425, 527
- Trujillo Bueno, J. & Manso Sainz, R. 1999, ApJ, 516, 436

Table 1: Wavelengths ( $\text{\AA}$ ) of  $F$ -state transitions for a hypothetical atomic system

	$F_b = 0$	$F_b = 1$	$F_b = 2$	$F_b = 3$
$F_a = 1$	5000.96093	5000.96075	5000.96036	N.A
$F_a = 2$	N.A	5000.98125	5000.98086	5000.98018

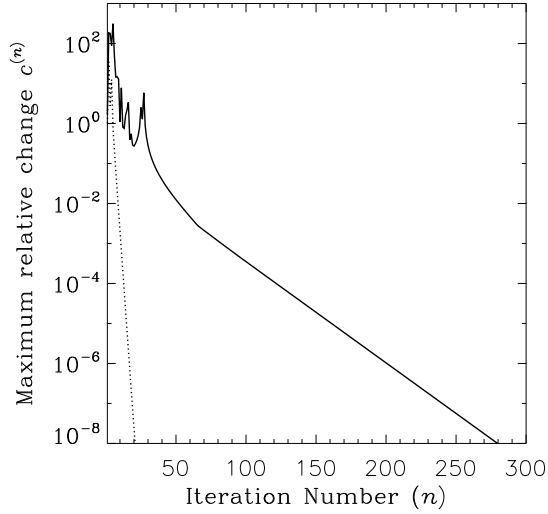


Fig. 2.— Comparison of PALI (solid line) and scattering expansion method (dotted line). The model parameters are given in the text. A convergence criteria of  $10^{-8}$  is used.

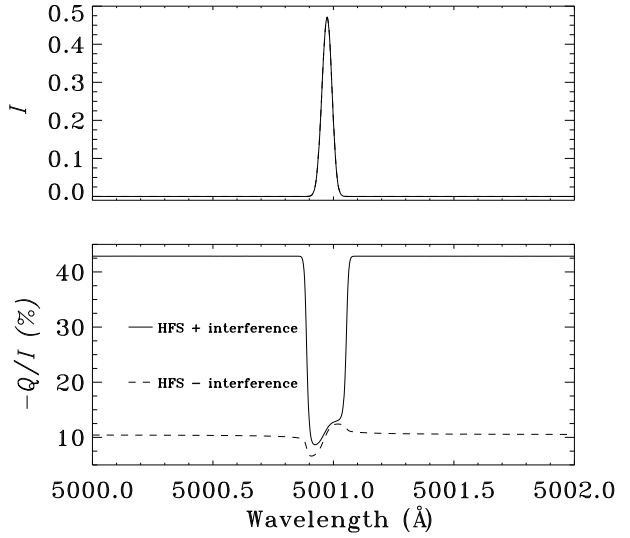


Fig. 3.— The profiles of the intensity  $I$  and the fractional polarization  $Q/I$ , plotted for a hypothetical line system with hyperfine structure splitting. Solid line represents the  $Q/I$  with  $F$ -state interference and dashed line represents  $Q/I$  without  $F$ -state interference. Single  $90^\circ$  scattering is assumed at the extreme limb ( $\mu = 0$ ). The model parameters are  $a = 0.002$ , the Doppler width  $\Delta\lambda_D = 0.025 \text{ \AA}$ .

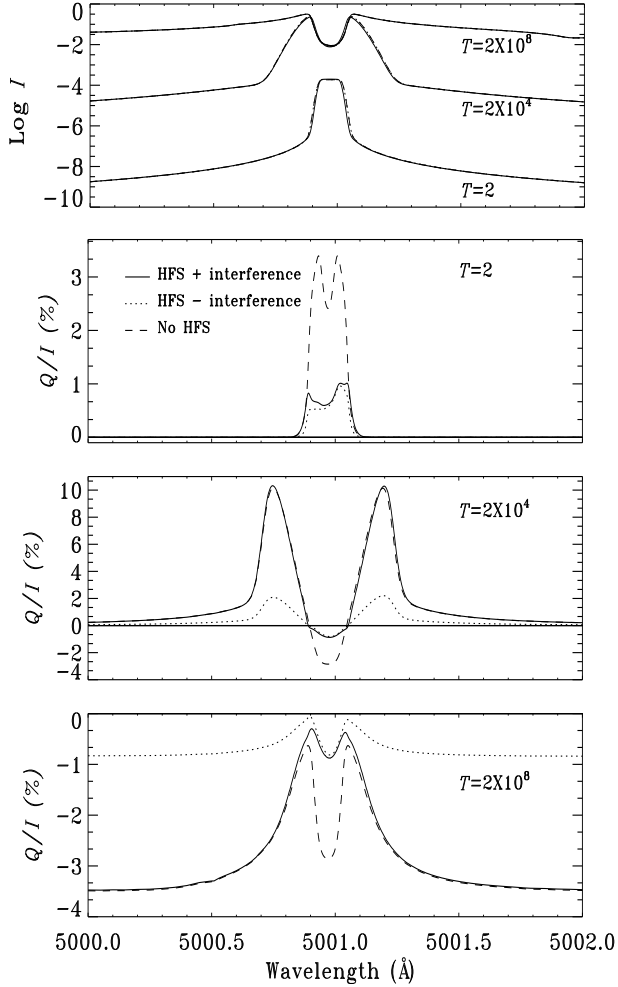


Fig. 4.— Comparison between the multiply scattered emergent Stokes profiles computed for different atomic systems as indicated in panel 2. The model parameters are  $(a, \epsilon, r, B) = (2 \times 10^{-3}, 10^{-4}, 0, 1)$ . The line of sight is given by  $\mu = 0.047$ . The wavelength positions of the six components are given in Table 1. The spacing between the hyperfine structure components is taken to be the same as those corresponding to the NaI D<sub>2</sub> line.

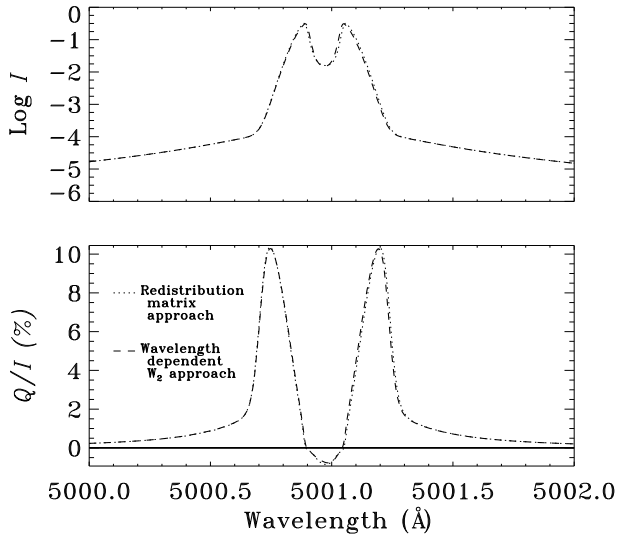


Fig. 5.— Comparison between the redistribution matrix theory (dotted line) and wavelength dependent polarizability factor  $W_2(\lambda)$  theory of Stenflo (dashed line). The optical thickness of the atmospheric slab is  $T = 2 \times 10^4$ . The other model parameters are the same as in Figure 4.